

Dynamic response analysis of ship-bridge collisions experiment^{*}

Jian GUO[†], Jing-xuan HE

Institute of Bridge Engineering, Zhejiang University of Technology, Hangzhou 310023, China

[†]E-mail: guoj@zjut.edu.cn

Received Aug. 14, 2019; Revision accepted Dec. 26, 2019; Crosschecked June 15, 2020

Abstract: Over the past decades, there has been continual construction of sea-crossing bridges as the technology of transportation improves. The probability of bridge pier being subjected to more vehicular impact is also growing. This study performed scale model tests and analyzed a collision mechanism considering the non-navigable span of a sea-crossing bridge in East China Sea as an engineering background. Comparing the test results with the finite element calculations, the dynamic response of the sample bridge and local damages of the fragile components under impact force were evaluated. Subsequently, the time-frequency characteristics of the vibration signal were analyzed based on wavelet packet analysis, and the multi-resolution characteristics as well as energy distribution of the vibration signal were discussed. It was observed that the impact energy transferred from ship to pier during the period of collision distributed different frequency bands with varying characteristics. The main frequency band (0–62.5 Hz) contains more than 75% of the vibration energy. The analysis can provide a basis for structural damage identification after the collision and anti-collision design of bridges.

Key words: Scaled model test; Ship collisions; Impact force; Wavelet packet analysis; Energy distribution
<https://doi.org/10.1631/jzus.A1900382>

CLC number: U447


1 Introduction

In recent years, with an increase in the construction of sea-crossing bridges around the world and the rise of sea-traffics, accidents resulting from ship-bridge collisions occur more frequently along waterways close to these bridges. For example, in 2007 a cargo ship bumped into the non-navigable pier of the Jiujiang Bridge resulting in the death of eight people in Guangdong, China (Fang et al., 2016). Also, in 2019 a cargo ship collided with non-navigable piers of Guang'anli Bridge in Busan, South Korea. In the design of bridges, ship collision force is an important load factor that must be considered. It is necessary to accurately predict the dynamic response of the bridge

structure and adequately design the bridge structure to resist the impact load. The dynamic analysis of bridge structure under ship impact is usually carried out by impact test which is the most authentic and credible method to study the ship-bridge collision problem. The experimental results are sufficient for providing necessary guidance for theoretical analysis, design of crashworthy structures, and verification of the results of numerical calculations.

As technology advances, many researchers have made a lot of achievements through experimental methods. In 1983, barge models of 1:6 and 1:4.5 proportions were used to carry out collision tests, and gravity-driven impact hammer was employed to gradually deform the barge bow of a European barge model. Through the analysis of the test results, the relationship between ship collision force, collision energy, and inelastic deformation was obtained (Meier-Dörnberg, 1983). The results of the tests provided an important reference for the formulation of ship collision specification formulas by the American

^{*} Project supported by the National Key Research and Development Program of China (No. 2018YFC0809604) and the National Natural Science Foundation of China (Nos. U1709207 and 51578506)

 ORCID: Jian GUO, <https://orcid.org/0000-0003-3605-2999>

© Zhejiang University and Springer-Verlag GmbH Germany, part of Springer Nature 2020

Association of State Highway and Transportation Officials in 1991 and 2014 (AASHTO, 2014). Full-scale barge impact tests were carried out at Robert C. Bird lock and dam near Gallipolis Ferry in West Virginia, USA. Although the test involves a small scale of bow deformation, it provides a useful insight into the impact behavior of the barge fleet (Patev, 2005). Arroyo-Caraballo and Ebeling (2006) used the energy method to interpret the impact data. A series of full-scale barge impact tests were carried out on two piers of St. George Island Embankment Bridge, USA. The structural dynamic response during the collision as well as the relationship between collision force and bow deformation was measured (Consolazio and Cowan, 2005). Sha and Hao (2012, 2013) studied the influence of various impact conditions (e.g. impact velocity, impact height, and bridge superstructure mass) using nonlinear finite element models (FEMs) of a barge bow and concrete column. Wang and Morgenthal (2017) proposed a dynamic model for barge impact, and Fan et al. (2008) combined FEM and artificial neural network for calculating the impact force. Through two kinds of tests, round pier and square pier impacting bow tests, the response of different types of piers to impact force was presented (Kantales et al., 2016). A refined bow model of an oil tanker was established at the ratio of 1:20 and also complemented with a static crush test. The static stiffness curve of the bow was presented. The test results provided an important reference for the relationship between bow deformation and impact force (Wan et al., 2019). Moreover, for both barge types, it was determined that a simplified elastic and entirely plastic barge force deformation relationship is relevant to bridge design (Consolazio et al., 2009). Demartino et al. (2017) studied the response of a shear-deficient circular reinforced concrete column under lateral impact loading by performing experimental tests, revealing the high vulnerability of these structural elements. Guo et al. (2017) proposed an optimal sensor placement method for damage detection of bridges after collisions. Wang et al. (2018) proposed a state-space model to identify the time lag between asynchronous accelerations at different positions during the collision of Jiangyin Bridge, China.

Previous ship collision tests usually focused on the relationship between ship collision force and bow deformation (Getter and Consolazio, 2011) as well as the dynamic response of piers. This study takes the

non-navigable span of a sea-crossing bridge in Zhejiang Province as the engineering background to carry out scaled model experiments and establish a precise FEM consisting of a pile foundation, cap, pier, and beam body. The magnitude of the impact force, dynamic response of each structure, and energy distribution of the bridge under impact with different velocities were analyzed, and the results of the experimental structure and the FEM were compared.

2 Experimental procedures

The establishment of the FEM and scaled model specimens will be introduced. Subsequently, the sensor arrangement and material characteristics of the test will be presented.

2.1 Ship bow

The idea of the reduced-scale test includes swinging a deformable bow into the concrete cap. The essential dimensions of the ship bow model are outlined in Fig. 1. The ship model was scaled in 1:20 and the weight of each bow replicated was approximately 16.6 kg. The bow model is mainly composed of an internal structure and external protective shell. The external protective shell was welded consisting of 1 mm steel plates. Because it is difficult to replicate every detail of the internal structure of the actual bow, the bow's internal structure was constructed with two equivalent brackets, which are also composed of steel. The ship bow model is shown in Fig. 2.

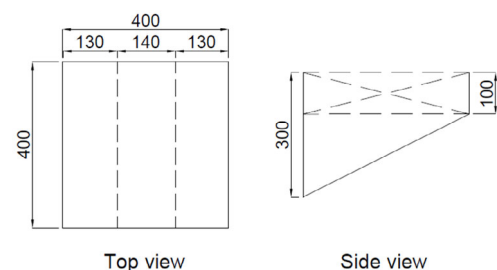


Fig. 1 Essential dimensions of the ship bow model (unit: mm)

2.2 Bridge specimens

Taking a non-navigable span of the Zhou-Dai sea-crossing bridge linking Zhoushan Island and Daishan Island in Zhejiang Province as an engineering

background, the ship-bridge collision test was carried out using a scale model. The non-navigable span of this bridge includes a 60-m prestressed-concrete continuous box girder. In order to study the same physical phenomena between the model and the prototype, it was necessary to make their stiffness basically the same. Therefore, the geometric size, boundary conditions, material properties, and motion conditions of the model must satisfy the relevant requirements. The overall model size was drawn to the scale of 1:20 of the actual bridge.

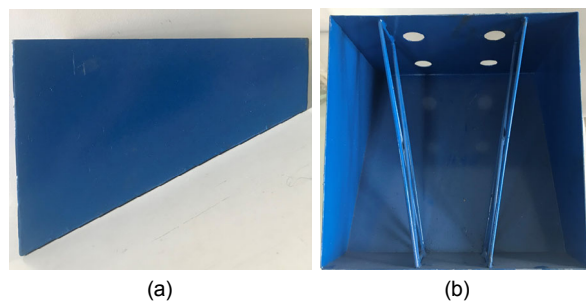


Fig. 2 Ship bow model
(a) Side view; (b) Bottom view

Under the condition of equivalent stiffness, the beam portion of the test model was designed as a T section. A circular steel pipe with a diameter of 89 mm and thickness of 2 mm was employed to simulate the steel pipe of the bridge pile foundation, and the pile length was 0.75 m which was determined using 8-time equivalent pile diameter method. In the model, concrete piers and caps were simulated by referring to the real bridge structure. As illustrated in Fig. 3b, steel bars were allocated according to the scale, and the thickness of the protective layer was suitably chosen. Fig. 4 visualizes the fabrication of the specimen. A rectangular rubber bearing (size: 150 mm×250 mm×42 mm) was installed between the beam and the pier to simulate the actual support under the beam of the sea-crossing bridge. The strength of the steel bar and steel pipe is Q335, and the concrete strength is C50. Specific measured parameters are outlined in Table 1.

2.3 Vibra-impact measure points

Importantly, it must be stated here that the sampling frequency of all the data was 1000 Hz. The main purpose of the test was to determine the ship collision force and the dynamic response of the scaled bridge

structure. Therefore, four force sensors were installed at the midpoint between the bow and the hull to record the time history curve of the impact force when the ship model collides with the bridge model. The reason for adopting four sensors was to eliminate the effect of bending moment. At the same time, in order to obtain the dynamic response of the bridge structure under the impact, nine accelerometers and 11 displacement sensors were installed in the cap, pier, pile foundation, and beam body as the sensor layout, illustrated in Fig. 5.

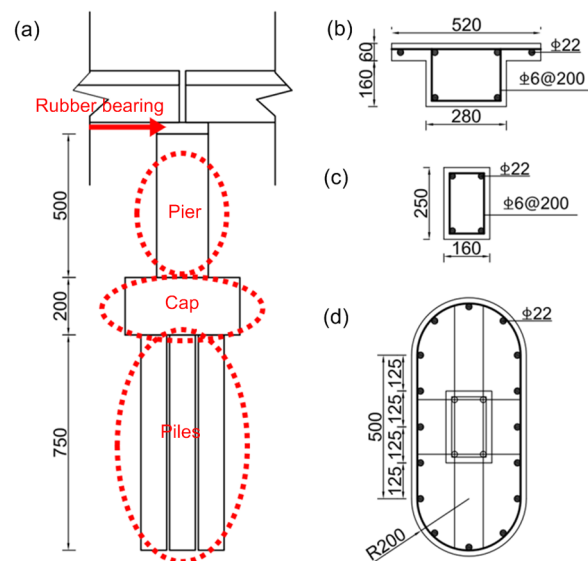


Fig. 3 Specimen dimensions (unit: mm)
(a) Elevation view; (b) Beam section; (c) Pier section; (d) Cap section

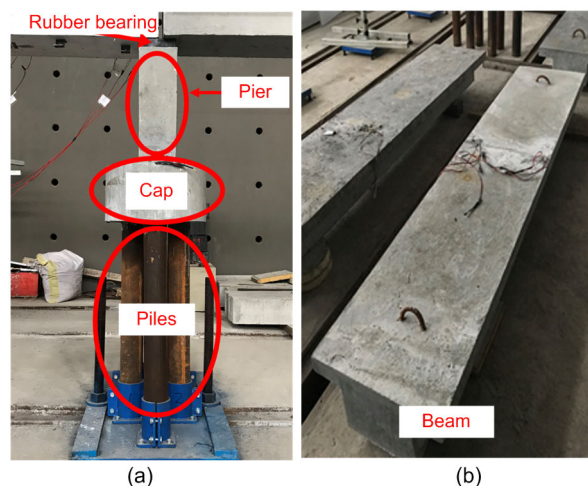
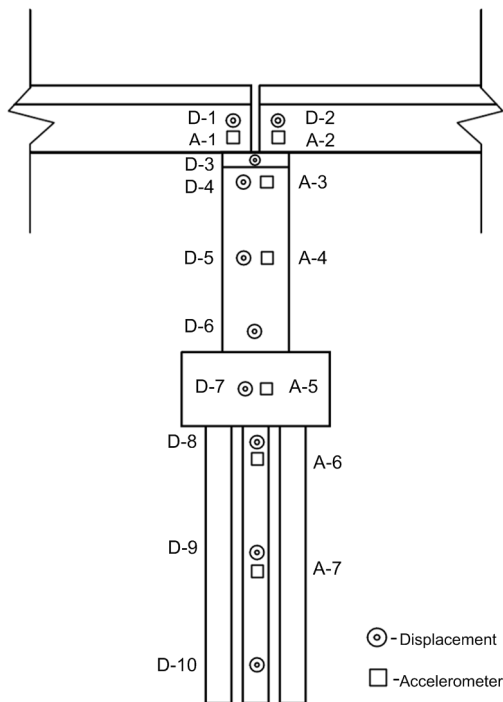


Fig. 4 Specimen fabrication
(a) Substructure; (b) Superstructure

Table 1 Material properties of bridge specimens

Member	Parameter	Value
Concrete	Density, ρ_c (kg/m ³)	2450
	Compressive strength, f_{cu} (MPa)	60.6
	Elastic module, E (MPa)	3.37×10^4
Rubber bearing	Morphological coefficient, S	8.06
	Friction coefficient, μ	≥ 0.3

**Fig. 5** Sensor layout of the bridge structure

3 Experimental results and analysis

According to the ship-bridge collision test outlined in Table 2, the test for the impact cap was divided into five groups which were set up using different velocities. From the test results, it was established that the damage mechanism and dynamic characteristics of concrete under these five working conditions were identical, so it was sufficient to compare and analyze one of them.

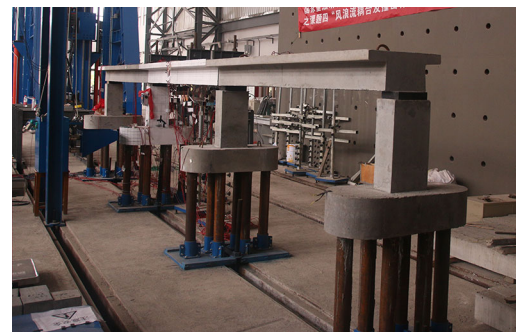
3.1 Finite element model

It is worthy of note at this juncture that a full-scale impact model has been established (Guo et al., 2019). An analysis was carried out using a non-

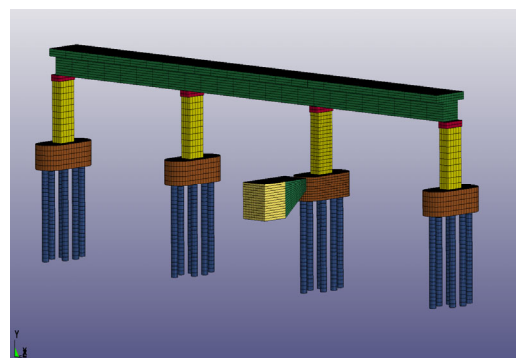
linear explicit dynamic finite element (FE) package (LS-DYNA) for numerical simulation before the experiment. After completing the physical test, the model was modified to conform to the exact conditions observed during the physical test (e.g. material properties of concrete and boundary conditions of bridges). Then, the modeling and simulation techniques were validated by comparing the results of impact simulation with the corresponding experimental data. Fig. 6a shows a field diagram of the experimental arrangement. Fig. 6b illustrates the FEM of the impact test which consists of 187410 elements. As shown in Fig. 7, the FEM and the test model have local damages near the impact points.

Table 2 Test conditions

Trial	Velocity (m/s)	Mass (kg)
T1	0.5	150.0
T2	1.0	150.0
T3	1.5	150.0
T4	2.0	150.0
T5	2.5	150.0



(a)



(b)

Fig. 6 Layout of the impact test (a) and the FEM (b)

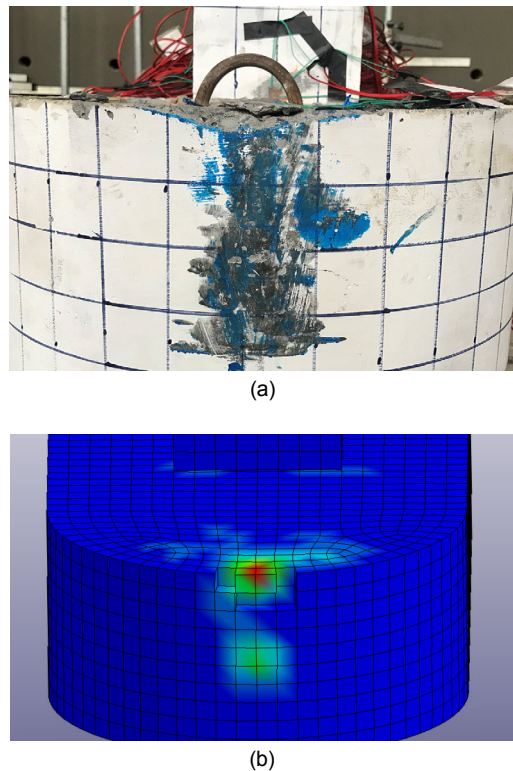


Fig. 7 Comparison of specimen damages between physical experiments (a) and FE simulations (b)

3.2 Impact force comparison

The force-time history curve of the impact test is shown in Fig. 8a. The largest impact velocity is 2.5 m/s, and the maximum test impact force is 19.8 kN, which occurs at 8 ms after impact. The duration and linearity of the impact force of the five groups were very similar. Fig. 8b displays the force-time history curve of the FEM, and Fig. 9 shows the comparison of the impact force between the test results and the FE results at 2.0 m/s. It is evident that there is a certain similarity between the experimental and numerical simulations of the impact force linearity. In terms of numerical value, the maximum impact force of the FEM and the test were 20.76 kN and 19.8 kN, respectively, and the error was less than 5%. It can be observed that the greater the velocity, the greater the maximum impact force and the longer the duration. At the same time, the peak value of the impact force clearly increases with the increase of velocity within 2.0 m/s. However, the peak impact force of the velocities within 2.0 m/s and 2.5 m/s does not change much. The results show that the impact

force can be explained using two stages: the rising stage and the plastic stage. As the bow makes contact with the cap, the impact force increases rapidly. Then, the bow undergoes plastic deformation and the impact force decreases.

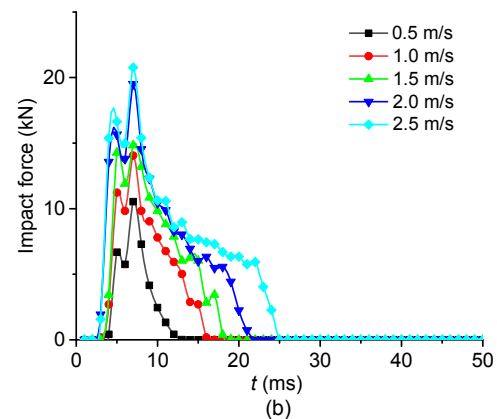
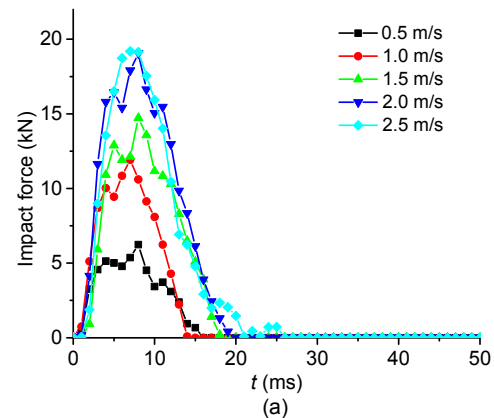


Fig. 8 Force-time history data for cap series
(a) Experimental results; (b) FEM results. t is the time

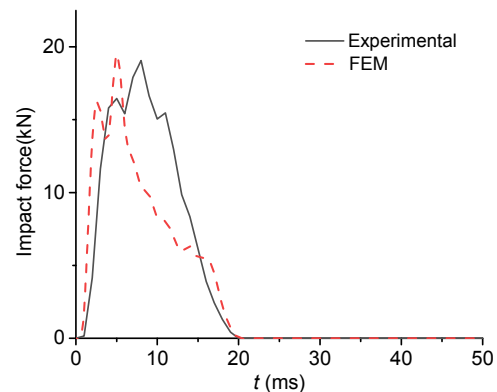


Fig. 9 Time-histories of impact force corresponding to FEM and experimental test at impact velocity of 2.0 m/s

3.3 Comparison of beam displacement

As demonstrated in Fig. 5, the data at measuring point D-1 at the edge of the beam were compared with the FE results. In the FEM, the friction coefficient between the beam and the rubber bearing was defined using the contact algorithm. The results at impact velocity of 1.0 m/s are shown in Fig. 10. From the figure, it is evident that the beam slips and vibrates when the substructure was impacted. When the beam was stabilized at an impact velocity of 2.0 m/s, the slip of the beam from the FEM can be observed to be 7.2 mm and that of the test was measured to be 8.32 mm. Fig. 11 shows the slip distance of the beam at different impact velocities. When the impact velocity was 2.5 m/s, the slip distance exceeded the range of the sensor; hence, no result was recorded at this velocity. The main factors affecting the slip distance are the magnitude of the impact force and the friction coefficient of the rubber bearing. However, the parameters of rubber bearings do not usually include friction coefficient and this deserves attention.

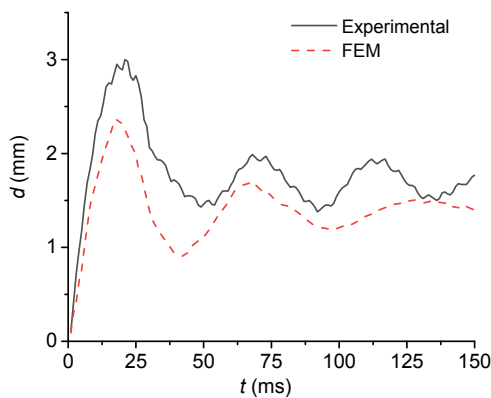


Fig. 10 Time-histories of beam displacement (d) corresponding to FEM and experimental test

3.4 Comparison of pier displacement

Because the pier top of the structure demonstrates the largest dynamic response, the displacement data of D-3 (Fig. 5) and the point measurement at the pier top position were compared. The results at impact velocities of 0.5 m/s and 1.0 m/s are shown in Fig. 12. The displacement measured at the remaining impact velocities was however not complete. It is evident from Fig. 12 that the maximum displacement measured from the experiment was 5.07 mm and was

4.56 mm from the FE result. The reason for a large experimental displacement value is that the base of the pile was riveted with grooved plates, on the other hand, the support connection for the numerical simulation was rigid hence a lower displacement value. As the flexibility of the test was lesser than that of numerical simulation, it was observed that the measured linear displacement was larger and the time to reach the peak value was longer.

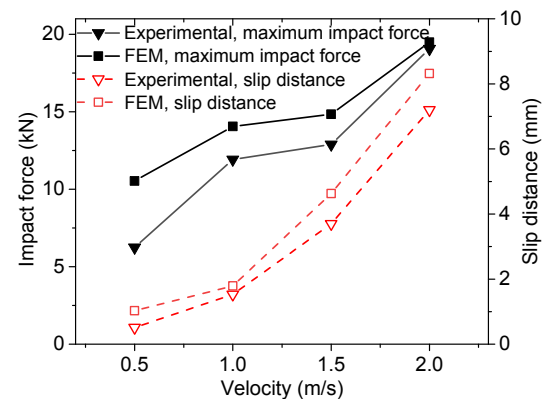


Fig. 11 Slip distance of beam at different impact forces and velocities

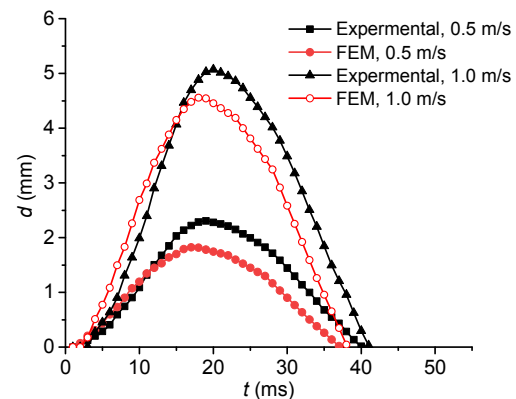


Fig. 12 Time-histories of pier displacement (d) corresponding to FEM and experimental test

3.5 Energy comparison of bridge components

During the ship-bridge collision, the kinetic energy of the ship hull was mainly absorbed in the form of bow deformation and by the bridge structure. From the FEM analysis, it was observed that the bridge structure absorbed the most energy at 0.004 s after the ship made contacts with the bridge. As illustrated in Fig. 13, at this time, the bow deformations absorbed

more than 80% of the energy. In the bridge structure, the most energy-absorbing section is the pile foundation. Significantly, the rubber bearings also accounted for approximately 3% of the energy. Therefore, as a fragile structure, the maintenance of bridges should be given considerable attention.

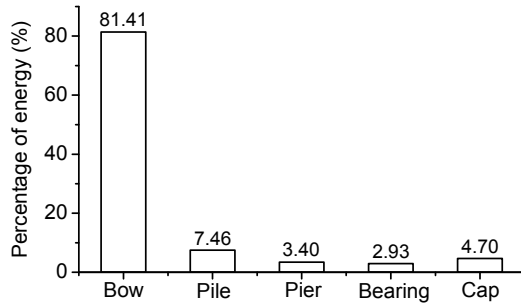


Fig. 13 Comparison of energy distribution for collision

4 Simulation results and discussion

The wavelet analysis method has an excellent localization property in both frequency and time domains (Graps, 1995). However, Fourier analysis is the only pure frequency analysis method. Wavelet analysis provides a flexible time-frequency window, which widens at low-frequency region and narrows at high-frequency region, and finally satisfies the demand of time-frequency analysis. These merits prove that wavelet analysis is better than Fourier analysis when evaluating non-stationary and non-periodic signals.

The vibration of the bridge due to ship impact constitutes a random signal. The acceleration of the cap and pier was collected under the impact condition with a velocity of 2.0 m/s. Then the acceleration data were modified using the wavelet transform to analyze the energy distribution on different scales. At present, db8 wavelet basis functions are widely used in the analysis of non-stationary vibration signals (Huang et al., 2019). In the wavelet analysis, besides choosing the appropriate basis function, the number of decomposition layers should also be determined. Assuming that the sampling frequency of the vibration signal is f_1 and the effective frequency range is $0-f_2$, the signal analysis frequency range is $0-f_1/2$. The impact vibration signal $S(t)$ was decomposed into i

layers by wavelet packet, and 2^i sub-bands can be obtained in layer i . The following is the expression of discrete wavelet packet:

$$S(t) = \sum_{j=0}^{2^i-1} f_{i,j}(t_j) \quad (1)$$

$$= f_{i,0}(t_0) + f_{i,1}(t_1) + \cdots + f_{i,2^i-1}(t_{2^i-1}),$$

where $f_{i,j}(t_j)$ is the reconstructed signal at the j th node of layer i .

According to Parseval theorem in signal spectrum analysis, the energy of the signal component in layer i is generally defined as

$$E_{i,j}(t_j) = \int |f_{i,j}(t_j)|^2 dt = \sum_{k=1}^m |x_{j,k}|^2, \quad (2)$$

where $E_{i,j}(t_j)$ represents the energy of the wavelet packet band at the j th node of layer i , m is the number of discrete sampling points, and $x_{j,k}$ is the amplitude of the reconstructed signal $f_{i,j}(t_j)$.

The original signal $S(t)$ is the sum of the reconstructed signals on all nodes in layer i , and the total energy of $S(t)$ is the sum of the energies of the signal components in layer i . The total energy E of the signal $S(t)$ can be obtained by

$$E = \sum_{j=0}^{2^i-1} E_{i,j}(t_j). \quad (3)$$

The ratio of the energy of each frequency band to the total energy of the analyzed signal is

$$P_{i,j} = \frac{E_{i,j}(t_j)}{E}. \quad (4)$$

In the modal test, the first two natural frequencies of the structure were 7.81 Hz and 19.53 Hz. The sampling frequency of the original acceleration signal of the platform was 1000 Hz, and the original signal was decomposed using four scales of wavelet. As visualized in Fig. 14, the original acceleration signal of the cap was analyzed using a wavelet packet, and the first four frequency bands of the reconstructed acceleration signal as shown in Fig. 15 were determined.

According to Eqs. (3) and (4), the energy ratio of each frequency band shown in Fig. 16a can be determined. Using the same method, the pier top acceleration and impact force were analyzed through wavelet packet analysis. The results are shown in Figs. 16b and 16c. Because the other bands have little energy, only a list of energy ratios of the first eight

bands is outlined in Table 3. It can be observed that more than 70% of the energy of the tested bridge structure was mainly distributed in the range of 0–62.50 Hz. Similarly, the energy of impact force was mainly concentrated in the low-frequency regime.

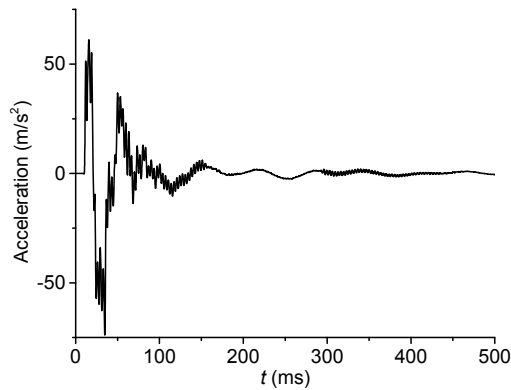


Fig. 14 Original acceleration signal of cap

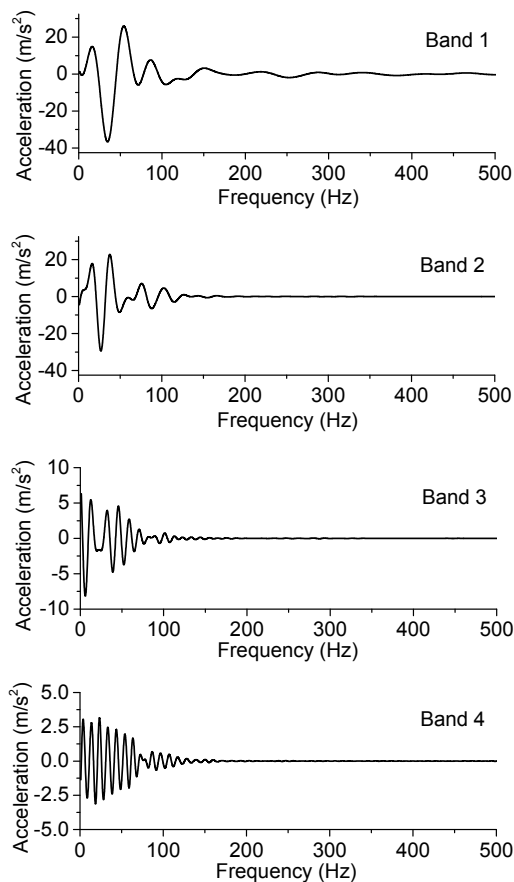


Fig. 15 Reconstructed acceleration signal of cap

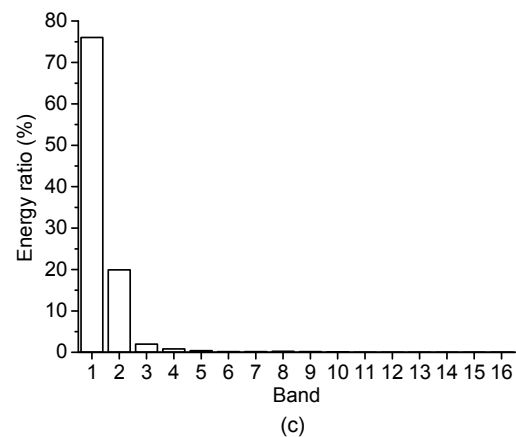
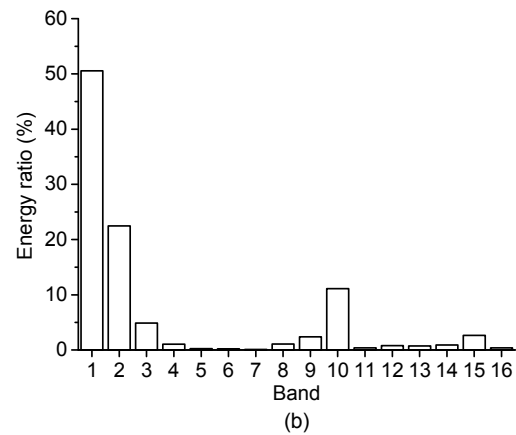
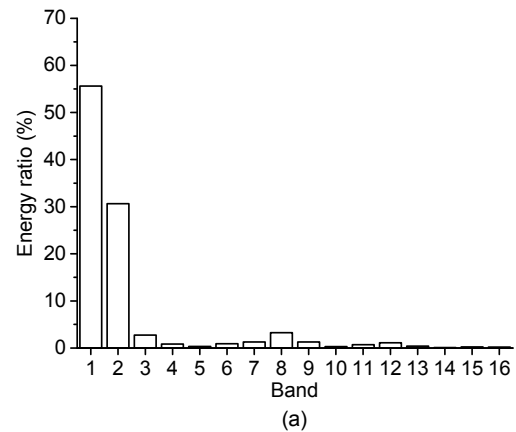


Fig. 16 Energy ratio of each frequency band after the wavelet packet decomposition

(a) Cap (A-5); (b) Pier top (A-3); (c) Impact force

Table 3 Energy ratios of the first eight bands after wavelet packet decomposition

Band	Frequency domain (Hz)	Energy ratio (%)		
		Cap	Pier top	Impact force
1	0–31.25	55.63	50.56	76.04
2	31.25–62.50	30.64	22.47	19.90
3	62.50–93.75	2.76	4.87	1.97
4	93.75–125.00	0.84	1.06	0.83
5	125.00–156.25	0.34	0.24	0.40
6	156.25–187.50	0.92	0.23	0.16
7	187.50–218.75	1.27	0.10	0.18
8	218.75–250.00	3.25	1.09	0.24

5 Conclusions

In this study, impact tests of the scaled bridge were performed. Five experiments were performed to evaluate the ship-bridge collision mechanism. An FE modeling method for impact response tests during the collision was proposed and validated. Based on the detailed experimental and numerical studies, the following conclusions were made:

1. The response of ship collision test with different impact velocities was compared and analyzed. The results show that the impact force can be explained in two stages: the rising stage and the plastic stage. In the first stage, the impact force rises abruptly to its maximum. During the second stage, the impact force decreases due to the plastic deformation of the bow.

2. A particular phenomenon that was generally ignored has been observed in the test. It is the relative displacement between the beam and pier due to the transverse inertial force. The maximum displacement in this experiment was 8.32 mm. In bridge design, the possibility of unseating superstructures should be considered after the pier is impacted.

3. During the ship-bridge collision, the ship absorbed most of the energy due to the deformation of the bow, which is more than 80% of the total energy. For bridge structures, most of the energy was concentrated on the deformation of the pile foundation and support.

4. Based on the analysis of the wavelet packet, it was observed that the energy absorbed by the tested bridge structure was mainly concentrated in the low-frequency band, in which the first two natural

frequencies of the structure were located. The analysis can provide a reference for structural damage identification and bridge design.

Contributors

Jian GUO designed the research. Jian GUO and Jing-xuan HE conducted the field test. Jing-xuan HE processed the corresponding data and wrote the first draft of the manuscript. Jian GUO and Jing-xuan HE revised and edited the final version.

Conflict of interest

Jian GUO and Jing-xuan HE declare that they have no conflict of interest.

References

- AASHTO (American Association of State Highway and Transportation Officials), 2014. AASHTO LRFD Bridge Design Specifications, 7th Edition. AASHTO, Washington DC, USA.
- Arroyo-Caraballo JR, Ebeling RM, 2006. Glancing-blow impact forces by a barge train on a lock approach wall. *Journal of Infrastructure Systems*, 12(2):135-143. [https://doi.org/10.1061/\(asce\)1076-0342\(2006\)12:2\(135\)](https://doi.org/10.1061/(asce)1076-0342(2006)12:2(135))
- Consolazio GR, Cowan DR, 2005. Numerically efficient dynamic analysis of barge collisions with bridge piers. *Journal of Structural Engineering*, 131(8):1256-1266. [https://doi.org/10.1061/\(asce\)0733-9445\(2005\)131:8\(1256\)](https://doi.org/10.1061/(asce)0733-9445(2005)131:8(1256))
- Consolazio GR, Davidson MT, Cowan DR, 2009. Barge bow force-deformation relationships for barge-bridge collision analysis. *Transportation Research Record*, 2131(1):3-14. <https://doi.org/10.3141/2131-01>
- Demartino C, Wu JG, Xiao Y, 2017. Response of shear-deficient reinforced circular RC columns under lateral impact loading. *International Journal of Impact Engineering*, 109:196-213. <https://doi.org/10.1016/j.ijimpeng.2017.06.011>
- Fan W, Yuan WC, Fan QW, 2008. Calculation method of ship collision force on bridge using artificial neural network. *Journal of Zhejiang University-SCIENCE A*, 9(5):614-623. <https://doi.org/10.1631/jzus.A071556>
- Fang H, Mao YF, Liu WQ, et al., 2016. Manufacturing and evaluation of large-scale composite bumper system for bridge pier protection against ship collision. *Composite Structures*, 158:187-198. <https://doi.org/10.1016/j.compstruct.2016.09.013>
- Getter DJ, Consolazio GR, 2011. Relationships of barge bow force-deformation for bridge design: probabilistic consideration of oblique impact scenarios. *Transportation Research Record*, 2251(1):3-15. <https://doi.org/10.3141/2251-01>
- Graps A, 1995. An introduction to wavelets. *IEEE Computational Science and Engineering*, 2(2):50-61. <https://doi.org/10.1109/99.388960>

- Guo J, Zheng YF, Song SY, 2019. Study on fluid-solid coupling of ship impact bridge considering tide level change. *Bridge Construction*, 49(6):24-29 (in Chinese).
- Guo YL, Ni YQ, Chen SK, 2017. Optimal sensor placement for damage detection of bridges subject to ship collision. *Structural Control and Health Monitoring*, 24(9):e1963. <https://doi.org/10.1002/stc.1963>
- Huang D, Cui S, Li XQ, 2019. Wavelet packet analysis of blasting vibration signal of mountain tunnel. *Soil Dynamics and Earthquake Engineering*, 117:72-80. <https://doi.org/10.1016/j.soildyn.2018.11.025>
- Kantrales GC, Consolazio GR, Wagner D, et al., 2016. Experimental and analytical study of high-level barge deformation for barge-bridge collision design. *Journal of Bridge Engineering*, 21(2):04015039. [https://doi.org/10.1061/\(ASCE\)BE.1943-5592.0000801](https://doi.org/10.1061/(ASCE)BE.1943-5592.0000801)
- Meier-Dörnberg KE, 1983. Ship collisions, safety zones, and loading assumptions for structures in inland waterways. *VDI-Berichte*, 496:1-9.
- Patev RC, 2005. Development of U.S. army corps of engineers engineering guidance for the barge impact design of navigation structures. *Transportation Research Record*, 1936(1):94-99. <https://doi.org/10.1177/0361198105193600111>
- Sha YY, Hao H, 2012. Nonlinear finite element analysis of barge collision with a single bridge pier. *Engineering Structures*, 41:63-76. <https://doi.org/10.1016/j.engstruct.2012.03.026>
- Sha YY, Hao H, 2013. Laboratory tests and numerical simulations of barge impact on circular reinforced concrete piers. *Engineering Structures*, 46:593-605. <https://doi.org/10.1016/j.engstruct.2012.09.002>
- Wan YL, Zhu L, Fang H, et al., 2019. Experimental testing and numerical simulations of ship impact on axially loaded reinforced concrete piers. *International Journal of Impact Engineering*, 125:246-262. <https://doi.org/10.1016/j.ijimpeng.2018.11.016>
- Wang W, Morgenthal G, 2017. Dynamic analyses of square RC pier column subjected to barge impact using efficient models. *Engineering Structures*, 151:20-32. <https://doi.org/10.1016/j.engstruct.2017.08.003>

- Wang WD, Jiang SF, Zhou HF, et al., 2018. Time synchronization for acceleration measurement data of Jiangyin Bridge subjected to a ship collision. *Structural Control and Health Monitoring*, 25(1):e2039. <https://doi.org/10.1002/stc.2039>

中文概要

题目: 船撞桥墩动力响应的试验研究

目的: 1. 研究船撞桥过程中撞击力的大小; 2. 在船撞作用下, 研究桥梁各结构的动力响应与脆弱部位; 3. 研究桥梁结构动力响应的频带特征以及能量分布。

创新点: 1. 通过缩尺试验和高分辨率的有限元模型, 探究船撞桥墩的碰撞机理; 2. 通过小波包分析方法, 对缩尺试验的敏感部位的响应进行分析, 探明其频带特性和能量分布。

方法: 1. 通过试验分析和有限元模拟, 找出桥墩的易损部位, 并研究速度与船舶刚度对撞击力大小的影响; 2. 通过精细化的有限元模型, 验证试验的准确性; 3. 在船撞作用下, 探究敏感部位的动力响应; 4. 通过小波包分析, 分解缩尺模型敏感部位的响应信号, 并研究其频带特性和能量分布。

结论: 1. 通过对不同撞击速度的船舶在碰撞时的冲击力与桥墩动力响应的研究表明, 撞击力可由上升段和塑性段两个阶段来解释。2. 当桥梁下部结构受到船舶撞击时, 支座与梁体会产生滑移; 因此, 在桥梁设计中应考虑船舶撞击引起落梁的可能。3. 在船撞过程中, 大部分能量被船舶的变形所吸收; 对于桥梁结构来说, 大部分能量集中在桩基与支座。4. 通过小波包分析可知, 桥梁结构吸收的能量主要集中在低频段。

关键词: 缩尺模型试验; 船撞桥墩; 冲击荷载; 小波包分析; 能量分布